JCTC Journal of Chemical Theory and Computation

Article

pubs.acs.org/JCTC

Costless Derivation of Dispersion Coefficients for Metal Surfaces

Neyvis Almora-Barrios,[†] Giuliano Carchini,[†] Piotr Błoński,[†,‡] and Núria López*[,†]

[†]Institute of Chemical Research of Catalonia, ICIQ, Av. Països Catalans 16, E-43007 Tarragona, Spain

[‡]Institute of Nuclear Physics, Polish Academy of Sciences, ul. Radzikowskiego 152, PL-31-342 Krakow, Poland

Supporting Information

ABSTRACT: Many common density functional theory methods used in the study of adsorption on metals lack dispersion contributions. Formulations like the random phase approximations would mitigate this error, but they are computationally too expensive. Therefore, semiempiric treatments based on dispersion coefficients turn out to be a practical solution. However, the parameters derived for atoms and molecules are not easily transferable to solids. In the case of metals, they cause severe overbinding as screening is not properly taken into consideration. Alternative ways to determine these parameters for metal surfaces have been put forward, but they are complex and not very flexible when employed to address low-coordinated atoms or alloys. In this work, we present a self-consistent, fast, and costless tool to obtain the dispersion coefficients for metals and alloys for pristine and defective surfaces. Binding energies computed with these parameters are compared to both the experimental and theoretical values in the literature thus demonstrating the validity of our approach.

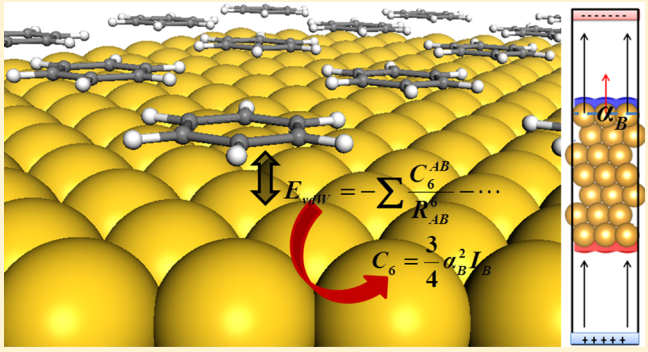

1. INTRODUCTION

Density functional theory (DFT) predicts many phenomena occurring on solid surfaces very successfully.[1] However, a serious shortcoming of the standard DFT based methods is that they do not account for van der Waals, vdW, interactions resulting from dynamical correlations between fluctuating charge distributions.[2] Thus, these calculations fail to reproduce the binding energies of the weakly interacting systems, e.g. organic molecules on metal surfaces.[3] In recent years, there has been a need to extend the applicability of the DFT-based methods to these new problems. We will discuss some of the main approaches that have been developed, but for more detailed discussion, we recommend refs 4−12.

The vdW interaction between an atom and a metal surface was understood to have a leading contribution of the type C_3/z^3 where z is the distance between the molecule and the surface.[13] The C_3 coefficients were then estimated from the polarizability of the molecule and the dielectric function of the surface derived from the Lifshitz formula.[14] This kind of approximation was used to estimate the contribution of these forces in the activation of methane on Ir(111).[15] However, the pair (molecule and surface) information contained in the C_3 parameter made it unpractical.

Alternatively, different functionals that include dispersion have been put forward. Lundqvist et al.[16−20] proposed a nonlocal correlation functional (vdW-DF) that accounts for dispersion interactions approximately. The results were found to depend on the particular combination between the exchange and the nonlocal correlation functionals (see, e.g., ref 21.). A formal rigorous alternative which includes the vdW energy seamlessly and accurately is offered by the random phase approximation (RPA),[22] combined with the adiabatic connection and fluctuation dissipation theorem (ACFDT)[23,24] as proposed by Kresse and Harl.[25−28] Unfortunately, it implies a heavy computational burden; hence it is more suitable for benchmarking than for extensive use, especially when studying reactivity of large molecules on metal surfaces.

On the other hand, the simplest correction is offered by the semiempirical contributions introduced by Grimme et al.[29] (DFT-D2). In this approach, the dispersion is calculated by pairwise interactions from the London formula[30] leading to a sum over C_6/R^6 terms. The C_6 parameters were tabulated for isolated atoms. Significantly, for the heavy atoms the same values were reported for a whole row of the periodic table. However, the DFT-D2 method with the coefficients derived from atomic properties leads to a substantial overbinding when applied to metals.[31] The natural evolution of the DFT-D2 method includes the next terms (C_8−C_{10}) in the expansion, DFT-D3.[32] In this approach there is a range of precalculated coefficients for various elements in different reference states. For instance, the C_6 coefficients are assigned to each pair of atoms taking into account the number of neighbors. Despite these improvements, the water−metal interaction is still largely overestimated.[33]

An alternative formulation, known as DFT-vdW[34] has been developed since by Tkatchenko−Scheffler (henceforth referred to as TS). In the TS method, the C_6 coefficients and radii are

Received: July 21, 2014
Published: September 29, 2014

   dx.doi.org/10.1021/ct5006467 | J. Chem. Theory Comput. 2014, 10, 5002−5009

determined nonempirically from the electron density, and effective atomic volumes are used to obtain environment dependency. However, it was not clear if the scaling of the coefficients with the volume would yield accurate results for more complex systems, such as metal surfaces.[35] A possible remedy, as Ruiz et al.[35] have pointed out recently, is to determine a metal surface C_6 coefficient that accounts for the collective response (screening) of the substrate electrons, by employing the Lifshitz–Zaremba–Kohn (LZK) theory[13,14] (DFT-vdW^{surf}). In this way the C_3- and C_6-based formulations can be mapped.[36] The method implies the use of frequency-dependent dielectric functions for transition metals from reflection electron energy-loss spectroscopy.[37] Therefore, the DFT-vdW^{surf} method to evaluate polarizabilities is not purely first principles.

The aim of this work is to elaborate an alternative for evaluating polarizabilities for atoms in both regular and defective metal surfaces and for unraveling the contribution from heterometallic bond formation in alloys only based on calculated data. From these data, we have derived the corresponding van der Waals coefficients. To test this approach, we present the results of benzene adsorption on a variety of metal surfaces, specifically on Pd, Pt, Cu, Ag, Au, and on bimetallic alloys and near-surface alloys (NSAs) containing Au. We have compared the experimental data to the results obtained with existing theoretical approaches by Grimme (DFT-D2 and DFT-D3), Tkatchenko and Scheffler (DFT-vdW^{surf}), and ours.

2. THEORETICAL BACKGROUND

In general, the interaction between two bodies A and B acting like isotropic oscillators is expressed in terms of dispersion coefficients, C_m:

$$E_{vdW}(R_{AB}) = -\frac{C_6}{R_{AB}^{\ 6}} - \frac{C_8}{R_{AB}^{\ 8}} - \dots \tag{1}$$

Since the interaction may be considered as taking place through a fluctuating electromagnetic field in each of the two bodies, the C_6 coefficient can be expressed as[38]

$$C_6 = \frac{3\hbar}{2\pi^2}\int_0^\infty d\omega \alpha_A(i\omega^I)\alpha_B(i\omega^I) \tag{2}$$

where $\alpha_A(i\omega^I)$ and $\alpha_B(i\omega^I)$ are the dynamic (frequency-dependent (ω), evaluated at imaginary frequencies) polarizabilities of the two subsystems. We follow the original procedure by London[30,37] who calculated the attraction between two atoms within second-order perturbation theory. London used the Unsöld approximation[39] to the second-order energy in which all the energy denominators can be replaced by some average value (the average excitation energies further approximated by the first ionization energies of the interacting subsystems). When acting on an alternating field of the effective frequency, these terms are described as follows:[30]

$$\alpha_A(i\omega^I) = \frac{\alpha_A(0)}{1 + (\omega^I/\omega_1)^2} \tag{3}$$

where ω_1 is the characteristic frequency and $\alpha_A(0)$ is the static polarizability. Having introduced this approximation in eq 2, the evaluation of the integral can be rewritten as

$$C_6 = \frac{3\hbar}{2}\alpha_A(0)\alpha_B(0)\frac{\omega_{1A}\omega_{1B}}{\omega_{1A} + \omega_{1B}} \tag{4}$$

Since the characteristic frequency multiplied by $\hbar$ is in all these cases near equal to the ionization energy I,[30] C_6 can be simplified to

$$C_6 = \frac{3}{2}\alpha_A(0)\alpha_B(0)\frac{I_A I_B}{I_A + I_B} \tag{5}$$

In the case of an ensemble of identical objects "B" eq 5 can be expressed as

$$C_6 = \frac{3}{4}\alpha_B(0)^2 I_B \tag{6}$$

and, thus the coefficient only depends on the static polarizability. For metals the surface static polarizability can be retrieved from the response of the dipole to the presence of an electric field as shown by Schneider and co.[40] The corresponding equation can be written:

$$\vec{\mu} = \sum_i^{surface} \vec{\mu}_i = \sum_i^{surface} \alpha_i(0)\vec{E} \tag{7}$$

where $\vec{\mu}$ is the total surface dipole moment that can be assigned to the individual atoms, $\vec{\mu}_i$. Further decomposition indicates that the individual dipoles (atom-in-surface model) depend on the atomic polarizabilities when applying an electric field $\vec{E}$, in our case in the direction perpendicular to the surface, see Figure 1. Note that the free electrons in the bulk of the metal

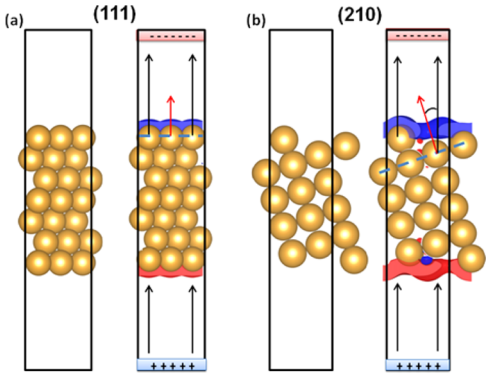

Figure 1. Side views of the surfaces of fcc metals and schematic representation of the method of imposing an electric field in surfaces where the electron spill is seen as electron density accumulation (blue) and depletion (red) on the surface: (111) the most densely packed surface (a) and (210) stepped surface (b).

show a zero frequency, i.e. do not contribute.[41] We consider that the main contribution to the bond to the surface would be due to the surface atoms, as dispersion forces show a $1/r^6$ dependence. The electric field can be introduced as a dipole sheet in the middle of the vacuum region, as proposed by Neugebauer and Scheffler[42] and the corresponding dipole can be obtained from the output of the DFT once the field is applied. The only limitation is that it should not be too strong to prevent spontaneous electron leakage from the surface and the metal-atoms rearrangement; its maximum values depend on the height of the supercell, as described below. The supercell dimensions used in this work allowed the use of electric fields up to (1 V Å^{-1}). Notice that only static polarizabilities and C_6 values corresponding to surface atoms can be obtained in this manner. The so-computed C_6 values are completely compatible

dx.doi.org/10.1021/ct5006467 | J. Chem. Theory Comput. 2014, 10, 5002−5009

with those derived from Grimme, as radii are very similar (see below) and the same damping function is employed.

The same methodology can be applied to different surface configurations like those presenting steps; see Figure 1b. In the particular case of a stepped surface, polarization of surface atoms is not as effective since the volume where electrons can polarize is not where the electric field drives them to. Thus, the angle formed between the electric field and surface normal needs to be taken into account. The total surface dipole can be decomposed considering that the atoms in low-index planes keep the polarizabilities obtained from the low-index surface calculations. Therefore, we have

$$\vec{\mu} = \sum_{i}^{\text{surface}} \vec{\mu}_i = \sum_{i}^{\text{surface}} \alpha_i(0)\vec{E}\hat{n} \tag{8}$$

where now $\hat{n}$ is the vector normal to the surface.

3. COMPUTATIONAL DETAILS

All calculations were based on density functional theory with periodic boundary conditions, using VASP code.[43−45] A basis set of plane waves, the generalized gradient approximation (GGA) and the Perdew−Burke−Ernzerhof (PBE) functional[46] were included. The interaction between valence and core electrons was described by the Projected Augmented Wave (PAW) method.[43] The number of plane waves was controlled by setting the cutoff energy to 400 eV. The metal surfaces were represented by different slab thickness, separated by 12 Å vacuum. In all cases, optimizations were performed for the two topmost layers where the rest were kept fixed to mimic the bulk. The corresponding k-point samplings were denser than 0.3 Å^{-1}.

An external electric field perpendicular to the slab was imposed using the method proposed by Neugebauer and Scheffler[42] as implemented in VASP.[47] The electric fields used were 0 to ±1 V Å^{-1} in four different steps of 0.25 V Å^{-1} size. The dipole moments were calculated by numerically integrating the charge density difference between a neutral slab and a slab with an applied electric field multiplied by the integration distance, following the procedure described by Schneider and co-workers.[40] The surface dipole can be written as

$$\vec{\mu} = qd\hat{n} \tag{9}$$

where q is the differential charge between the slab with and without electric field and d is the distance in angstroms. q is obtained by integration of the charge density assigned to the surface metal atom, from the midpoint between the surface, z_{1L}, and subsurface layer, z_{2L}, thus $(z_{1L} - z_{2L})/2$ to the point where the density difference is zero $z_{\Delta\rho=0}$:

$$q = \int_{z_{1L}-z_{2L}/2}^{z_{\Delta\rho=0}} \Delta\rho(z)\, \mathrm{d}z \tag{10}$$

and

$$d = z_{\text{total}}\left(z_{q=0} - \frac{z_{1L} - z_{2L}}{2}\right) \tag{11}$$

Tests of the convergence of the dipole moments with respect to the slab thickness were done (see in Supporting Information Table-S1). For the simplest surfaces, the variation of the dipole moment was then plotted against an applied electric field and the slope divided by the number of surface atoms corresponds to the polarizability, $\alpha(0)$. Then the C_6 coefficient was obtained by using the atomic ionization potentials I from the Handbook.[48] In each case, the radius, R_0, corresponds to half of the distance between two neighboring atoms in the relaxed bulk (see Table S-2). The obtained values are in line with those reported earlier in the literature.[35] The parameters for the molecules and the damping function were taken from those early reported by Grimme.[29]

4. RESULTS AND DISCUSSION

4.1. Polarizabilities and Dispersion Coefficients. The difference in electronic charge density between a neutral slab and one with the electric field imposed is showed in Figure 2.

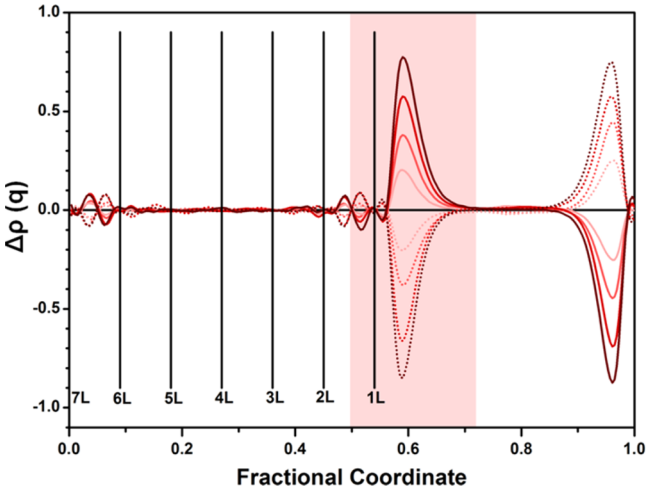

Figure 2. Plane-averaged electronic charge difference between a bare seven layer Au(111) slab calculated with and without external field. Vertical lines stand for the positions of the Au layers and the area of integration is in pink background.

The surface atoms are the only ones affected by the excess of the charge as it would be expected for a metal. They polarize in opposite sign on either side of the slab. We have then calculated the dipole using eq 9 for fcc (111) metal surfaces.

The dipole moment as a function of the electric field is plotted in Figure 3. A linear relation between the dipole and the imposed field is found and the slope directly represents the

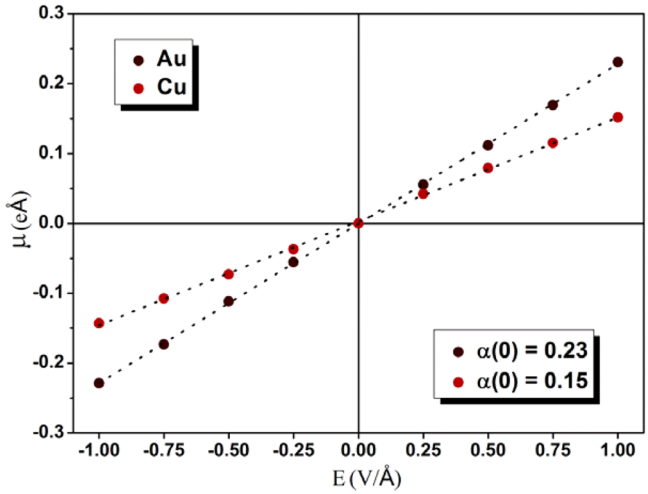

Figure 3. Au(111) and Cu(111) dipole moments as a function of the external electric field. The slope corresponds to the polarizabity in eÅ^2/V.

dx.doi.org/10.1021/ct5006467 | J. Chem. Theory Comput. 2014, 10, 5002−5009

Table 1. Polarizabilities (α, bohr^3) for the Atom[a]

M (111)	α_{atom}[48]	α_{cal}	α_{LZK}[35]	C_6^{atom}	C_6^{cal}	$C_6^{DFT\text{-}vdW^{surf}}$[35]	$C_6^{DFT\text{-}D2}$[29]	$C_6^{DFT\text{-}D3}$[32]
Ni	45.9	14.7		447	46		189	129
Pd	32.4	19.5	13.9	243	88	102	432	266
Pt	43.9	19.5	14.5	478	94	120	1409	337
Cu	41.2	14.9	10.9	363	48	59	189	175
Ag	48.6	21.4	15.4	497	96	122	432	269
Au	39.1	22.4	15.6	392	128	134	1409	317

[a]From the Handbook for the isolated atom, α_{atom} our values for surface atom α_{cal}; and LZK from Tkatchenko−Scheffler α_{LZK}. Dispersion coefficients (C_6, hartree bohr^6) for the atom C_6^{atom}; our values C_6^{cal}; those from TS $C_6^{DFT\text{-}vdW^{surf}}$; and Grimme $C_6^{DFT\text{-}D2}$ and $C_6^{DFT\text{-}D3}$; parameters are also shown for comparison.

static polarizability $\alpha(0)$, according to eq 7. These atomic polarizabilities are significantly smaller than those obtain for the isolated metal atoms; see Table 1. The embedding environment thus acts by reducing the effect of the field in the surface atoms as most of the atomic density is compromised in forming bonds to the rest of the metal atoms. In general, we have found that the polarizability is around a 30% of the free atom value for Cu and Ni and around 60% for the rest. The metal $\alpha(0)$ increases with the Z number (for instance Ni vs Pd or Pt), but they are similar within the same period (compare Ni vs Cu values) as suggested by Grimme in his first tabulated data.[29] When compared to the LZK-derived α the values are slightly larger, about 25%, but the values from LZK correspond to bulk atoms.[35]

Using eq 6 the C_6 parameters for all the metals were obtained. Our results are presented in Table 1 and compared to other data in the literature. The present C_6 parameters are smaller than those of the free atoms or the DFT-D2 or DFT-D3 formulations, in some cases by even an order of magnitude. In contrast, the values are rather close to the values derived by TS.

4.2. Benchmark: Adsorption of Benzene. To evaluate the quality of these new coefficients, we proceeded to calculate the binding energy, BE, of benzene on the (111).[49] This energy is defined in such a way that an exothermic process yields a positive value:

$$\mathrm{BE} = -(E_{\mathrm{Surf+Bz}} - E_{\mathrm{Surf}} - E_{\mathrm{Bz}}) \tag{12}$$

Benzene is particularly suitable for testing weak interactions, as it is a large closed-shell molecule with aromatic electrons likely to be polarized. For this reason a large amount of data regarding benzene adsorption on a wide variety of surfaces is available for comparison. For the sake of comparison we employed the supercell reconstruction (3 × 3) for the (111) metal facet and the configuration for benzene from previous computational investigations; for Ag, Au, and Cu, this corresponds to hcp30°, while for Pd and Pt, it is bri30°, see inset Figure 4.[35,37] For the active metals Pd and Pt a dense phase with a p(4 × 4) supercell and two benzene rings was proposed,[31] and this better represents the experimental high coverage regime for which temperature-programmed desorption, TPD, values exist.[38,50−55] The results obtained have been represented in Figure 4 and summarized in Table 2, along with a PBE calculation, the Grimme approaches DFT-D2,[29] DFT-D3,[32] and DFT-vdW^{surf},[35,37] and experimental values. The binding energies were recalculated through the Redhead equation from TPD data,[39] employing both a default prefactor of 10^{13} or a entropy-corrected one (υ_{CS}), following the procedure of Campbell and Sellers.[56]

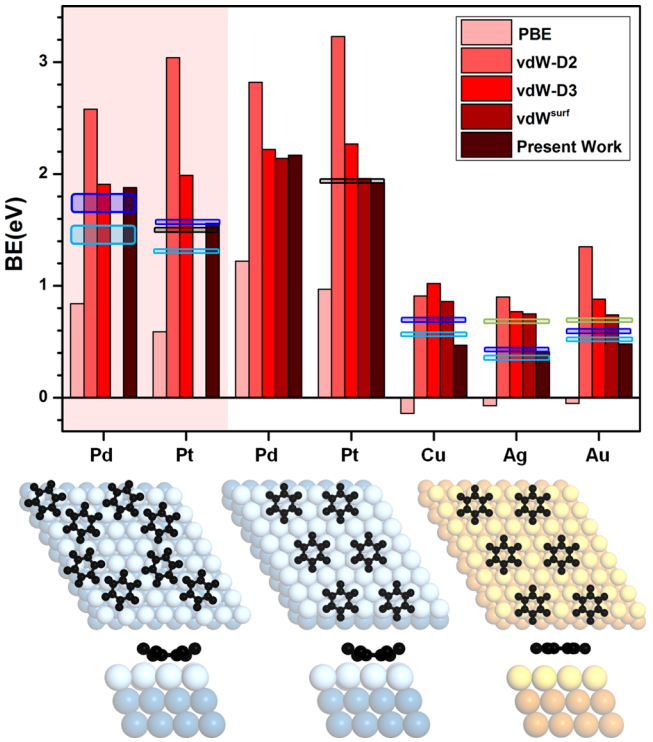

Figure 4. Binding energy (BE, in eV) for benzene on the (111) of different metals. The figure shows the comparison between different methodologies: PBE, Grimme DFT-D2 and DFT-D3 methods, DFT-vdW^{surf}, and the one developed in this work. The shaded area corresponds to high coverage models. The experimental values estimated from TPD data are shown by light ($\upsilon = 10^{13}$) and dark (υ_{CS} = corrected prefactor)[56] blue areas. The estimates from experiments derived in ref 37 are marked by green shaded areas. For C_6H_6/Pt(111), we report microcalorimetric measurements in black.

For Cu, Ag, and Au, benzene is weakly physisorbed. PBE leads to endothermic adsorption and DFT-D2 leads to severe overbinding that is not mitigated with DFT-D3, which results in adsorption energies larger for Cu than for Au, at odds with the experimental ordering. DFT-vdW^{surf} yields values close to the experimental ones, with slight overestimation. In turn, our method provides slightly lower estimates than the experiments. The energy differences between experiments and our data are largest for Cu and in excellent agreement for Au and Ag.

In turn, Pt and Pd are characterized by a strong chemisorptions, thus in the TPD experiments a rather large coverage appears about 0.095 ML.[31] Again PBE underestimates the values while DFT-D2 and DFT-D3 overestimate adsorption. Even in this case, the calculated adsorption energy

Table 2. Binding Energies (BE, eV) for the Adsorption of Benzene on Different Metal Surfaces[a]

metal	PBE	DFT-D2	DFT-D3	DFT-vdW^{surf} [37]	this work	exp
			$M(4 \times 4) + 2C_6H_6$			
Pd	0.84	2.58	1.91		1.88	1.64[31]−1.83[50]
Pt	0.59	3.04	1.99		1.57	1.54[52]−1.60[51] (1.54)[57]
			$M(3 \times 3) + C_6H_6$			
Pd	1.22	2.82	2.22	2.14	2.17	
Pt	0.97	3.23	2.27	1.96	1.92	(1.94)[57]
Cu	0.14	0.91	1.02	0.86	0.47	0.70[53]−0.71[38]
Ag	0.07	0.90	0.77	0.75	0.41	0.46[58]−0.45[54]
Au	0.05	1.35	0.88	0.74	0.48	0.63[55]

[a]The experimental values estimated from TPD data are reported via an entropy-corrected prefactor.[56] For C_6H_6/Pt(111) we report microcalorimetric measurements in parentheses. The Ag data[54,58] corresponds to the shoulder that appears at the same coverage as our calculations were performed, 140 K. There is another higher temperature peak at lower coverages 205 K. The TPD data from Au[55] shows a high energy peak that continuously shifts from 239 to 175 K, thus the assignment is unclear.

is reversed from experiments thus leading to qualitative inaccuracies. In comparison, our method slightly overestimates the interaction respect to the experimental value. In the isolated regime represented by the $p(3 \times 3)$ supercell our results are very close to those of DFT-vdW^{surf}. Experimentally, more accurate data have been reported by Campbell and Sellers[56] for benzene adsorption on Pt(111) at low and high coverage (marked in black in Figure 4). Our estimates are within 0.1 eV error when compared the microcalorimetric values.

4.3. Structural Defects: Steps and Other Low-Coordinated Sites. Open surfaces containing atoms with low coordination numbers and/or structural defects might be responsible for the adsorption and activation of molecules. We have studied how polarizabilities and coefficients vary as a function of the facet exposed.[59−61]

The total dipole moment is generated by the contributions from the dipoles assigned to the individual atoms on the surface. Geometric considerations describe the total dipole moments considering that terrace atoms form an angle with the field; see Figure 5. We have determined the dipole moment for the (100), (110), and (210) surfaces from the DFT calculations. We have then investigated if the polarizability of the atoms only depends on the coordination number and thus the results from the low-index facets can be used to simplify the equations and to obtain the values for each atom on the surface. Table 3 shows the variation of both the static polarizability and the vdW coefficient with the coordination number of surface atoms.

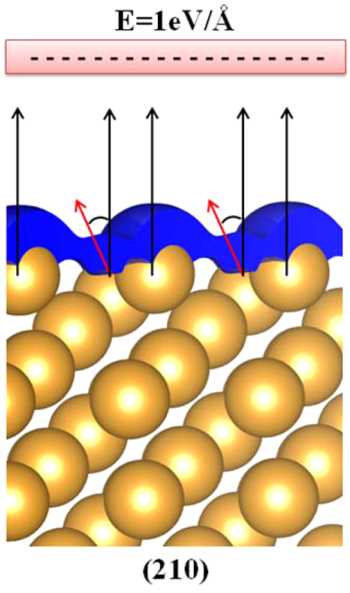

Figure 5. Schematic representation of the electron spill toward the vacuum by the electric field perpendicular to the edge of the step. The different orientation with the natural dipoles of the individual atoms is shown for clarity.

Table 3. Polarizabilities and Dispersion Coefficients as a Function of Coordination Number

	α (bohr^3)				C_6 (hartree bohr^6)			
	(111)	(100)	(110)	(210)	(111)	(100)	(110)	(210)
M	$N_c = 9$	$N_c = 8$	$N_c = 7$	$N_c = 6$	$N_c = 9$	$N_c = 8$	$N_c = 7$	$N_c = 6$
Ni	14.7	15.3	25.3	37.3	46	50	136	296
Pd	19.5	20.4	25.3	42.1	88	97	148	410
Pt	19.5	20.1	27.2	43.8	94	101	184	476
Cu	14.9	16.1	22.6	34.5	48	56	110	254
Ag	21.4	23.3	35.9	50.6	96	115	273	538
Au	22.4	23.3	35.0	48.6	128	140	314	606

The values found indicate that the polarization is larger when reducing the coordination number and it keeps the low values for 3d metals and higher ones for the rest. This variation has a second effect on the vdW coefficient which increases quite dramatically (almost 50 times) from the (111) facet to the coordination 6 of atoms at the steps of the (210) surface.

These variations with the Z number and the coordination can be summarized in a clearer way that allows us to understand the origin of the modulation of the C_6 parameter. Tkatchenko et al. suggested in ref 35 that the void volume surrounding an atom at the surface would imply a change in its polarizability as the electrons would be able to spill to a larger volume. This is clearly shown from our reported polarizabilities and C_6 parameters in Figure 6. To analyze the dependence we have defined the void volume, V, as follows:

$$V = (12 - N_c)V_{at}$$

where N_c is the coordination number of the atom and 12 represents its number of first neighbors in an fcc metal and V_{at} is the atomic volume. The calculated coordination-dependent polarizabilities are found to depend linearly on the void volume as shown in Figure 6−top. Correspondingly, the C_6 value follows quadratic dependence with the volume as it was put

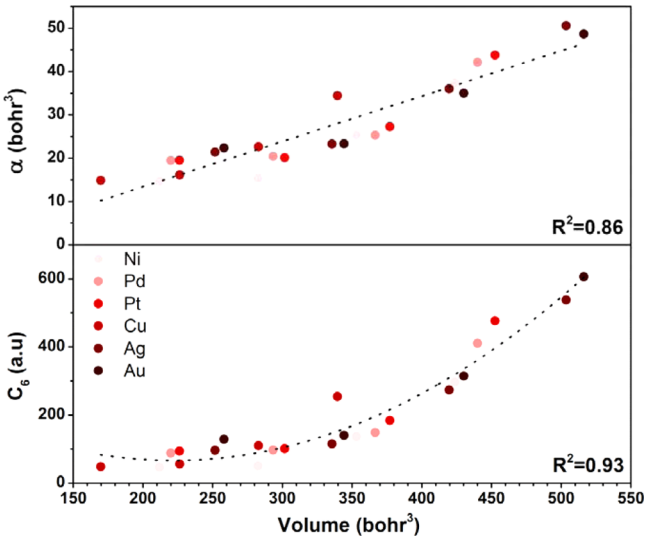

Figure 6. Polarizability as a function of volume of the exposed atoms $\alpha(0) = (0.105 \pm 0.009)V - 8 \pm 3$ and C_6 coefficient as a function of the exposed volume $C_6 = (0.0060 \pm 0.0009)V^2 + (-2.8 \pm 0.7)V + (372 \pm 108)$.

forward[35] initially but, more importantly, this dependence is found to be metal-independent.

4.4. Alloys. Our approach also allows the study of complexity in the form of alloys. In particular, we have derived C_6 parameters for overlayers and NSA; see Figure 7 for the

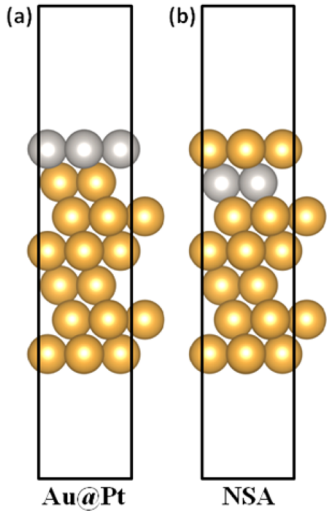

Figure 7. Schematic representation of the surfaces alloys Au@Pt (a) and NSA (b).

schematic representation. All these materials have proven their potential in catalysis and electrocatalysis.[1,62] In Figure 8, the results for different configurations of the Pd, Pt, Cu, Ag as overlayers, or NSA, are shown and compared to the pure metal values. Results indicate that the coefficients can vary more than 60%, the largest changes are obtained when smaller atoms are placed as overlayers on the surface. Au (Cu) can be taken as an example. This is again due to the change in the void volume. The correction is smaller for similar diameter atoms as overlayers (Pt). In turn, the changes do not affect the Au layer in the NSA models, again no modifications in volume are

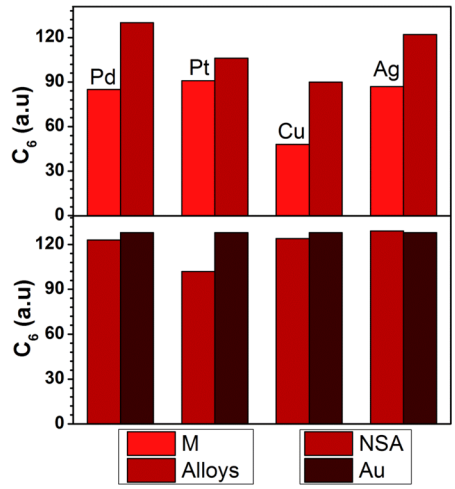

Figure 8. Dispersion coefficients (C_6, hartree bohr^6) for alloys and NSA. Metal pure parameters are also shown for comparison.

seen. The largest variation corresponds to Pt and correlates with the change in the position of the Fermi level for the NSA.

The contributions from the formation of the alloy indicate that adsorption does not significantly vary for many of the overlayers or alloys. Table 4 presents the test on benzene

Table 4. Binding Energies (BE, eV) for the Adsorption of Benzene (Bz) on Different Alloys and NSA Surfaces in the Isolated Molecule Configurations

metal	$BE^{C_6^M}$	$BE^{C_6^{alloy}}$	$BE^{C_6^{NSA}}$	$BE^{C_6^{Au}}$
Pd	2.23	2.37	0.50	0.48
Pt	2.26	2.29	0.49	0.48
Cu	0.50	0.67	0.33	0.48
Ag	0.44	0.51	0.48	0.48

adsorption. The largest variations observed are about 0.1−0.2 eV and correspond to the large increase in the value of C_6 for Cu on the overlayer and the concomitant reduction for the NSA. The enhancement is also found for Pd and Ag overlayers on Au.

5. CONCLUSIONS

van der Waals contributions are fundamental to obtain accurate estimates of the adsorption energies of large molecules on metals. Although robust ways of obtaining these energies are being developed, many of them are very computationally demanding and practical implementations would benefit from semiempirical approaches that can reduce the computational burden. For the interaction with metals, we have developed a method based on the determination of static polarizabilities that together with the ionization potentials provide reliable values for the C_6 coeffients for surface atoms. This simple model based on the response to an electric field can be applied to low-coordinated centers and alloys. In order to test the so-derived coefficients benzene adsorption energies have been taken as benchmark. Our results indicate that the method is robust and provides accurate results. In addition, a general dependence for the C_6 coeffients with the void volume, i.e. the volume where the electronic cloud can spill, has been found and can be employed as a fast estimate of coefficients for other metals. Finally, our values are compatible with already well-established contributions from atoms and molecules from Grimme's

dx.doi.org/10.1021/ct5006467 | J. Chem. Theory Comput. 2014, 10, 5002−5009

approach as it shares with this method the damping functions and follows radius definition. In addition, our results show excellent agreement with experimental determinations, in particular with the microcalorimetric measurements by Campbell and co. Finally, we consider that our costless, simple yet efficient tool can be a guide to extend the use of van der Waals contributions to different surface−adsorbate problems.

■ ASSOCIATED CONTENT

Supporting Information

Slab thickness convergence tests, atom radii, detailed TPD−computational adsorption energy comparisons. This material is available free of charge via the Internet at http://pubs.acs.org/.

■ AUTHOR INFORMATION

Corresponding Author

*E-mail: nlopez@iciq.es.

Notes

The authors declare no competing financial interest.

■ ACKNOWLEDGMENTS

This research has been supported by the ERC Starting Grant (ERC-2010-StG-258406), and we thank BSC-RES for providing us with generous computational resource. We are grateful to Dr. R. Valero (Ulsan National Institute of Science and Technology, Korea) for useful discussions.

■ REFERENCES

(1) Nørskov, J. K.; Bligaard, T.; Rossmeisl, J.; Christensen, C. H. Towards the computational design of solid catalysts. *Nat. Chem.* **2009**, *1*, 37−46.

(2) Hafner, J. Ab-initio simulations of materials using VASP: Density-functional theory and beyond. *J. Comput. Chem.* **2008**, *29*, 2044−2078.

(3) Mercurio, G.; McNellis, E. R.; Martin, I.; Hagen, S.; Leyssner, F.; Soubatch, S.; Meyer, J.; Wolf, M.; Tegeder, P.; Tautz, F. S.; Reuter, K. Structure and Energetics of Azobenzene on Ag(111): Benchmarking Semiempirical Dispersion Correction Approaches. *Phys. Rev. Lett.* **2010**, *104*, 036102.

(4) von Lilienfeld, O. A.; Tavernelli, I.; Rothlisberger, U.; Sebastiani, D. Optimization of Effective Atom Centered Potentials for London Dispersion Forces in Density Functional Theory. *Phys. Rev. Lett.* **2004**, *93*, 153004.

(5) Johnson, E. R.; Becke, A. D. A post-Hartree−Fock model of intermolecular interactions. *J. Chem. Phys.* **2005**, *123*, 024101.

(6) Tkatchenko, A.; Romaner, L.; Hofmann, O. T.; Zojer, E.; Ambrosch-Draxl, C.; Scheffler, M. Van der Waals interactions between organic adsorbates and at organic/inorganic interfaces. *MRS bull.* **2010**, *35*, 435−442.

(7) Steinmann, S. N.; Corminboeuf, C. A generalized-gradient approximation exchange hole model for dispersion coefficients. *J. Chem. Phys.* **2011**, *134*, 044117.

(8) Mackie, I. D.; DiLabio, G. A. Interactions in Large, Polyaromatic Hydrocarbon Dimers: Application of Density Functional Theory with Dispersion Corrections. *J. Phys. Chem. A* **2008**, *112*, 10968−10976.

(9) Sato, T.; Nakai, H. Density functional method including weak interactions: Dispersion coefficients based on the local response approximation. *J. Chem. Phys.* **2009**, *131*, 224104.

(10) Gräfenstein, J.; Cremer, D. An efficient algorithm for the density-functional theory treatment of dispersion interactions. *J. Chem. Phys.* **2009**, *130*, 124105.

(11) Silvestrelli, P. L.; Benyahia, K.; Grubisiĉ, S.; Ancilotto, F.; Toigo, F. Van der Waals interactions at surfaces by density functional theory using Wannier functions. *J. Chem. Phys.* **2009**, *130*, 074702.

(12) Klimeš, J.; Michaelides, A. Perspective: Advances and challenges in treating van der Waals dispersion forces in density functional theory. *J. Chem. Phys.* **2012**, *137*, 120901.

(13) Zaremba, E.; Kohn, W. Van der Waals interaction between an atom and a Solid-Surface. *Phys. Rev. B* **1976**, *13*, 2270−2285.

(14) Lifshitz, E. M. The theory of molecular attractive forces between solids. *Sov. Phys.−JETP* **1956**, *2*, 73−83.

(15) Henkelman, G.; Jónsson, H. Theoretical Calculations of Dissociative Adsorption of CH_4 on an Ir(111) Surface. *Phys. Rev. Lett.* **2001**, *86*, 664−667.

(16) Lee, K.; Murray, E. D.; Kong, L.; Lundqvist, B. I.; Langreth, D. C. Higher-accuracy van der Waals density functional. *Phys. Rev. B* **2010**, *82*, 081101.

(17) Dion, M.; Rydberg, H.; Schroder, E.; Langreth, D. C.; Lundqvist, B. I. Van der Waals density functional for general geometries. *Phys. Rev. Lett.* **2004**, *92*, 246401.

(18) Dion, M.; Rydberg, H.; Schroder, E.; Langreth, D. C.; Lundqvist, B. I. Erratum: Van der Waals Density Functional for General Geometries [Phys. Rev. Lett. 92, 246401 (2004)]. *Phys. Rev. Lett.* **2005**, *95*, 109902.

(19) Andersson, Y.; Langreth, D. C.; Lundqvist, B. I. van der Waals Interactions in Density-Functional Theory. *Phys. Rev. Lett.* **1996**, *76*, 102−105.

(20) Langreth, D. C.; Lundqvist, B. I.; Chakarova-Käck, S. D.; Cooper, V. R.; Dion, M.; Hyldgaard, P.; Kelkkanen, A.; Kleis, J.; Lingzhu, K.; Shen, L.; Moses, P. G.; Murray, E.; Puzder, A.; Rydberg, H.; Schröder, E.; Thonhauser, T. A density functional for sparse matter. *J. Phys.−Condens. Mater.* **2009**, *21*, 084203.

(21) Hamada, I.; Otani, M. Comparative van der Waals density-functional study of graphene on metal surfaces. *Phys. Rev. B* **2010**, *82*, 153412−153412−4.

(22) Nozières, P.; Pines, D. Correlation Energy of a Free Electron Gas. *Phys. Rev.* **1958**, *111*, 442−454.

(23) Dobson, J. F.; Dinte, B. P. Constraint Satisfaction in Local and Gradient Susceptibility Approximations: Application to a van der Waals Density Functional. *Phys. Rev. Lett.* **1996**, *76*, 1780−1783.

(24) Furche, F.; Van Voorhis, T. Fluctuation-dissipation theorem density-functional theory. *J. Chem. Phys.* **2005**, *122*, 164106.

(25) Harl, J.; Kresse, G. Accurate Bulk Properties from Approximate Many-Body Techniques. *Phys. Rev. Lett.* **2009**, *103*, 056401.

(26) Harl, J.; Schimka, L.; Kresse, G. Assessing the quality of the random phase approximation for lattice constants and atomization energies of solids. *Phys. Rev. B* **2010**, *81*, 115126.

(27) Lebègue, S.; Harl, J.; Gould, T.; Ángyán, J. G.; Kresse, G.; Dobson, J. F. Cohesive Properties and Asymptotics of the Dispersion Interaction in Graphite by the Random Phase Approximation. *Phys. Rev. Lett.* **2010**, *105*, 196401.

(28) Schimka, L.; Harl, J.; Stroppa, A.; Grüneis, A.; Marsman, M.; Mittendorfer, F.; Kresse, G. Accurate surface and adsorption energies from many-body perturbation theory. *Nat. Mater.* **2010**, *9*, 741−744.

(29) Grimme, S. Semiempirical GGA-type density functional constructed with a long-range dispersion correction. *J. Comput. Chem.* **2006**, *27*, 1787−1799.

(30) London, F. The general theory of molecular forces. *Trans. Faraday Soc.* **1937**, *33*, 8b−26.

(31) Tysoe, W. T.; Ormerod, R. M.; Lambert, R. M.; Zgrablich, G.; Ramirez-Cuesta, A. Overlayer structure and kinetic behavior of benzene on palladium(111). *J. Phys. Chem.* **1993**, *97*, 3365−3370.

(32) Grimme, S.; Antony, J.; Ehrlich, S.; Krieg, H. A consistent and accurate ab initio parametrization of density functional dispersion correction (DFT-D) for the 94 elements H-Pu. *J. Chem. Phys.* **2010**, *132*, 154104.

(33) Tonigold, K.; Groß, A. Dispersive interactions in water bilayers at metallic surfaces: A comparison of the PBE and RPBE functional including semiempirical dispersion corrections. *J. Comput. Chem.* **2012**, *33*, 695−701.

(34) Tkatchenko, A.; Scheffler, M. Accurate Molecular Van Der Waals Interactions from Ground-State Electron Density and Free-Atom Reference Data. *Phys. Rev. Lett.* **2009**, *102*, 073005.

(35) Ruiz, V. G.; Liu, W.; Zojer, E.; Scheffler, M.; Tkatchenko, A. Density-Functional Theory with Screened van der Waals Interactions

for the Modeling of Hybrid Inorganic-Organic Systems. *Phys. Rev. Lett.* **2012**, *108*, 146103.
(36) Liu, W.; Tkatchenko, A.; Scheffler, M. Modeling Adsorption and Reactions of Organic Molecules at Metal Surfaces. *Acc. Chem. Res.* **2014**, Article ASAP.
(37) Wei, L.; Victor, G. R.; Guo-Xu, Z.; Biswajit, S.; Xinguo, R.; Matthias, S.; Alexandre, T. Structure and energetics of benzene adsorbed on transition-metal surfaces: density-functional theory with van der Waals interactions including collective substrate response. *New J. Phys.* **2013**, *15*, 053046.
(38) Lukas, S.; Vollmer, S.; Witte, G.; Wöll, C. Adsorption of acenes on flat and vicinal Cu(111) surfaces: Step induced formation of lateral order. *J. Chem. Phys.* **2001**, *114*, 10123−10130.
(39) Redhead, P. A. Thermal desorption of gases. *Vacuum* **1962**, *12*, 203−211.
(40) Deshlahra, P.; Wolf, E. E.; Schneider, W. F. A Periodic Density Functional Theory Analysis of CO Chemisorption on Pt(111) in the Presence of Uniform Electric Fields. *J. Phys. Chem. A* **2009**, *113*, 4125−4133.
(41) Feynman, R. P.; Leighton, R. B.; Sands, M. L. Refractive Index of Dense Materials. In *The Feynman Lectures on Physics: Mainly electromagnetism and matter*; Gottlieb, M. A., Pfeiffer, P., Eds.; Addison-Wesley: California, 1965; Vol. *II*.
(42) Neugebauer, J.; Scheffler, M. Adsorbate-substrate and adsorbate-adsorbate interactions of Na and K adlayers on Al(111). *Phys. Rev. B* **1992**, *46*, 16067−16080.
(43) Kresse, G.; Joubert, D. From ultrasoft pseudopotentials to the projector augmented-wave method. *Phys. Rev. B* **1999**, *59*, 1758−1775.
(44) Kresse, G.; Furthmuller, J. Efficiency of ab-initio total energy calculations for metals and semiconductors using a plane-wave basis set. *Comput. Mater. Sci.* **1996**, *6*, 15−50.
(45) Kresse, G.; Furthmuller, J. Efficient iterative schemes for ab initio total-energy calculations using a plane-wave basis set. *Phys. Rev. B* **1996**, *54*, 11169−11186.
(46) Perdew, J. P.; Burke, K.; Ernzerhof, M. Generalized gradient approximation made simple. *Phys. Rev. Lett.* **1996**, *77*, 3865−3868.
(47) Feibelman, P. J. Surface-diffusion mechanism versus electric field: Pt/Pt(001). *Phys. Rev. B* **2001**, *64*, 125403.
(48) *CRC Handbook of Chemistry and Physics*, 84 ed.; Lide, D. R., Ed.; CRC Press: 2003; p 2616.
(49) Liu, W.; Carrasco, J.; Santra, B.; Michaelides, A.; Scheffler, M.; Tkatchenko, A. Benzene adsorbed on metals: Concerted effect of covalency and van der Waals bonding. *Phys. Rev. B* **2012**, *86*, 245405.
(50) Waddill, G. D.; Kesmodel, L. L. Benzene chemisorption on palladium surfaces. I. High-resolution electron-energy-loss vibrational spectra and structural models. *Phys. Rev. B* **1985**, *31*, 4940−4946.
(51) Campbell, J. M.; Seimanides, S.; Campbell, C. T. Probing ensemble effects in surface reactions. 2. Benzene adsorption on clean and bismuth-covered platinum(111). *J. Phys. Chem.* **1989**, *93*, 815−826.
(52) Xu, C.; Tsai, Y. L.; Koel, B. E. Adsorption of cyclohexane and benzene on ordered tin/platinum (111) surface alloys. *J. Phys. Chem.* **1994**, *98*, 585−593.
(53) Xi, M.; Yang, M. X.; Jo, S. K.; Bent, B. E.; Stevens, P. Benzene adsorption on Cu(111): Formation of a stable bilayer. *J. Chem. Phys.* **1994**, *101*, 9122−9131.
(54) Rockey, T. J.; Yang, M.; Dai, H.-L. Adsorption Energies, Inter-adsorbate Interactions, and the Two Binding Sites within Monolayer Benzene on Ag(111). *J. Phys. Chem. B* **2006**, *110*, 19973−19978.
(55) Syomin, D.; Kim, J.; Koel, B. E.; Ellison, G. B. Identification of Adsorbed Phenyl (C_6H_5) Groups on Metal Surfaces: Electron-Induced Dissociation of Benzene on Au(111). *J. Phys. Chem. B* **2001**, *105*, 8387−8394.
(56) Campbell, C. T.; Sellers, J. R. V. The Entropies of Adsorbed Molecules. *J. Am. Chem. Soc.* **2012**, *134*, 18109−18115.
(57) Ihm, H.; Ajo, H. M.; Gottfried, J. M.; Bera, P.; Campbell, C. T. Calorimetric Measurement of the Heat of Adsorption of Benzene on Pt(111). *J. Phys. Chem. B* **2004**, *108*, 14627−14633.
(58) Meserole, C. A.; Vandeweert, E.; Postawa, Z.; Haynie, B. C.; Winograd, N. Energetic Ion-Stimulated Desorption of Physisorbed Molecules. *J. Phys. Chem. B* **2002**, *106*, 12929−12937.
(59) Vilé, G.; Baudouin, D.; Remediakis, I. N.; Copéret, C.; Lõpez, N.; Pérez-Ramírez, J. Silver nanoparticles for olefin production: New insights into the mechanistic description of propyne hydrogenation. *ChemCatChem.* **2013**, *5*, 3750−3759.
(60) Almora-Barrios, N.; Novell-Leruth, G.; Whiting, P.; Liz-Marzán, L. M.; López, N. Theoretical Description of the Role of Halides, Silver, and Surfactants on the Structure of Gold Nanorods. *Nano Lett.* **2014**, *14*, 871−875.
(61) Vilé, G.; Almora-Barrios, N.; Mitchell, S.; López, N.; Pérez-Ramírez, J. From the Lindlar Catalyst to Supported Ligand-Modified Palladium Nanoparticles: Selectivity Patterns and Accessibility Constraints in the Continuous-Flow Three-Phase Hydrogenation of Acetylenic Compounds. *Chem.—Eur. J.* **2014**, *20*, 5926−5937.
(62) Greeley, J.; Mavrikakis, M. Alloy catalysts designed from first principles. *Nat. Mater.* **2004**, *3*, 810−815.